MODULAR APPLICATION OF MOVING-BELT PLASMA-FACING COMPONENTS FOR PARTICLE AND HEAT REMOVAL FROM A STEADY-STATE FUSION SYSTEM

Y. Hirooka and M. S. Tillack
Fusion Energy Research Program
Department of Applied Mechanics and Engineering Sciences
University of California, San Diego
9500 Gilman Dr., La Jolla, CA 92093-0417

ABSTRACT

Discussed in this report is the possibility of modular application of moving-belt plasma-facing components for a steady-state magnetic fusion device. Individual modules will provide specific functions such as particle control and heat removal. Modular-by-modular operational windows concerning belt length, moving speed, plasma exposure length and surface temperature have been analyzed in detail.

I. INTRODUCTION

Much has been discussed on the handling of particle and heat fluxes onto plasma-facing components (PFCs) over the past two decades. New physics concepts for edge control and innovative technologies for heat removal have been developed along with the ITER design effort [1] and with advanced fusion experiments [2]. However, not enough attention has been directed to "true" steady-state PFC issues. Steady-state operation requires continuous impurity control for plasma cleanliness, recovery of tritium for fuel recycle, and removal of heat for power generation. For conventional PFCs, however, periodic shutdown for maintenance is unavoidable, for example, in order to replace eroded surface components and/or rejoin with the heat sink structure, etc.

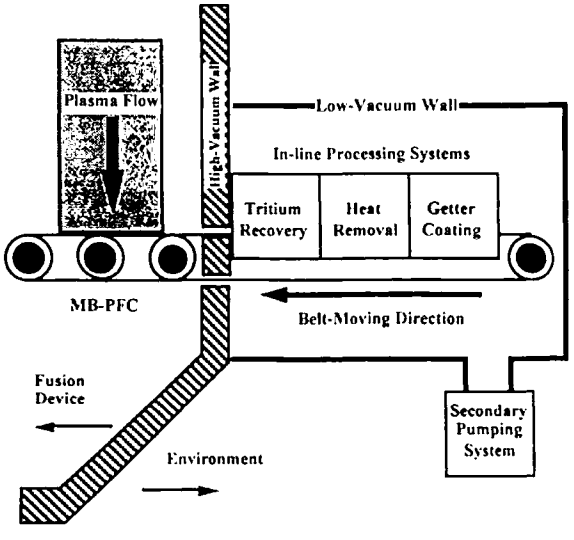

Fig. 1 The moving-belt PFC concept with ex-situ inline belt regeneration systems for tritium recovery, heat removal and getter coatings [3].

In our recent work [3], as shown in Fig. 1, the use of moving-belt plasma-facing components (MB-PFCs) with ex-situ belt regeneration systems for continuous impurity gettering, heat removal and tritium recovery has been proposed. In order to minimize MHD effects and induced radioactivity, semi-conductor materials such as SiC-fiber fabrics are considered for the belt. These fibers are woven without binder, so that the resultant fabrics remain flexible. To compensate for the gas leak through the belt openings, the regeneration systems may be housed in a low vacuum enclosure. Imporatnatly, MB-PFCs can be applied for all types of magnetic fusion devices whether or not in the full toroidal configuration.

The MB-PFC system performance has been evaluated in case studies under selected reactor relevant conditions, similar to those listed in Table 1. It is found that the belt erosion rate is diluted over the total belt area and is independent of moving speed. Non-saturable impurity gettering is possible under zero-erosion conditions. Heat removal can be carried out continuously either by radiative cooling or contact conductance. High-efficiency tritium recovery can be maintained for long-term (~ 100 years) operation, mitigating the impact on environmental safety.

Proposed in this report is modular application of MB-PFCs, meaning that a toroidal fusion device is installed with two or more MB-PFC modules, operating under the optimized conditions for their respective functions such as particle control and heat removal. This modular approach will avoid over-expectations like one configuration for all functions, the traditional PFC technology dilemma.

II. MB-PFC MODULE FOR PARTICLE CONTROL

A. Steady-state impurity gettering

To briefly review our recent work [3], the erosion rate of MB-PFCs is related to that of conventional PFCs in the following manner:

$$\Gamma_{MB\text{-}e} = \Gamma_e(\ell_p/L) \qquad (1)$$

where $\Gamma_{MB\text{-}e}$ is the erosion rate of a moving belt, Γ_e is the erosion rate of a standing surface component, ℓ_p is the plasma interaction length and L is the total belt length. The erosion rate is "diluted" over the moving surface by a factor of (ℓ_p/L) and independent of belt speed.

Also, it has been demonstrated that unlimited lifetime MB-PFCs can be achieved by coating the belt with gettering materials such as Li, Be, and B at the same rate as they may be eroded during plasma exposure. The coatings deposition rate is given by the following relation:

$$\Gamma_{MB-d} = \Gamma_d(\ell_d/L)\phi(\theta)\nu \qquad (2)$$

where Γ_{MB-d} is the deposition rate on a moving belt, Γ_d is the deposition rate on a standing belt, ℓ_d is the length of the coating section, $\phi(\vartheta)$ is the correction factor for the viewing angle, ϑ, and ν is the trapping coefficient. Notice that the aerial dilution factor, (ℓ_d/L), appears in eq. (2), too.

Under the conditions listed in Table 1, TRIM.SP [4] calculations indicate that C, O-impurities will be trapped at the efficiency of 100% by Li, Be, B getters as long as the surface implanted layer is unsaturated. The effective impurity deposition flux on a moving belt is estimated from eq. (2), setting $\phi(\vartheta)=1$, $\nu=1$, and $\ell_d = \ell_p$. Here, we define the degree of saturation in getter coatings as follows:

$$\eta = \frac{(\ell_p/v)(\ell_p/L)\Gamma_{in}}{(R/d_a)N_s} \qquad (3)$$

where η is the degree of saturation, v is the belt speed, Γ_{in} is the incoming particle flux, R is the implantation range, d_a is the atomic spacing, and N_s is the monolayer atomic density. The factors, (ℓ_p/v) and (R/d_a), will thus give the plasma exposure time and the number of monolayers in the range, respectively. We assume that C, O-impurities will be gettered 100% (i.e., $\nu=1$) as long as $\eta \le \eta_{max\text{-}i} = 0.5$, above which gettering is prevented due to the formation of compounds such as Li_2O and/or B_4C. For simplicity, the maximum saturation is assumed not to vary with temperature.

B. Steady-state fuel particle pumping

The rate of loss of particles from a fusion system at steady-state is given by the following relation [5]:

$$\Gamma_{loss} = \frac{Vn_e}{\tau_p} \qquad (4)$$

where Γ_{loss} is the D, T-particle loss rate, V is the total plasma volume, n_e is the averaged plasma density, and τ_p is the global particle confinement time. To remove these particles, the pumping system must meet the condition:

$$S_p = \frac{\Gamma_{loss}}{P} \qquad (5)$$

where S_p is the pumping speed, and P is the neutral pressure. From the conditions in Table 1, one finds that $\Gamma_{loss} = 5 \times 10^{22}$ DT particles/s, i.e., 1.5×10^{3} Torr ℓ s. Although it depends on the operational scenario, the edge neutral pressure is assumed to be of the order of 10^{-3} Torr. This leads to the requirement that $S_p = 1.5 \times 10^{6}$ ℓ/s, which is extremely difficult to be maintained for steady-state operation. In the case of ITER [1], a large number of cryo pumps are designed to operate in an alternating mode: one group in operation and the other under regeneration.

As such, steady-state particle removal is a key issue affecting the operational scenario. Generally, the pumping speed is restricted by gas conductance. Many existing fusion devices are equipped with large turbo molecular pumps and/or cryo pumps but in severely limited conductance configurations for protecting the inlet structure from high energy particle bombardment. On the other hand, it is well known that the first wall materials such as graphite often provide more pumping effects than actual pumps. This is because the first wall has a larger surface area and can tolerate direct bombardment of high energy plasma particles. By nature, however, these wall pumping effects are saturable and need to be regenerated.

The possibility of using MB-PFCs is thus evaluated next as a pump to remove fuel particles at steady-state. Here, we assume that the degrees of saturation in getter-coatings as to hydrogenic species and impurities are independent of each other. Hydrogenic species are assumed to be trapped 100% as long as $\eta \le \eta_{max\text{-}f} = 0.4$, the data widely accepted for graphite [8]. Compared with hydride stoicheometries such as LiH_2, this is a very conservative assumption. It is important to mention that the saturation level remains unchanged up to about 500 °C but decreases exponentially as temperature increases above this point.

Table 1 Case study MB-PFC operating conditions.

Total plasma volume, V	1000 m^3
Averaged plasma density, n_e	10^{20} m^{-3}
Global particle confinement time, τ_p	2 s
Divertor footprint total area, $A_{div.}$	5 m^2
Edge neutral pressure, P	10^{-3} Torr
Impurity-to-fuel plasma flux ratio	0.01
Particle bombarding energy, E	100 eV
Averaged plasma heat flux, $<q_p>$	1 MW/m^2
Belt length, L	20 m
Plasma interaction length, ℓ_p	0.5 m
Belt width, w	1 m
Belt speed, v	2 m/s
Belt thickness, t_b	5 mm
Belt density, ρ	2.2 g/cm^3
Belt temperature during exposure	500 °C (Module-I) 1000 °C (Module-II)
Belt surface emissivity, ε	0.8
Thermal conductivity ($\perp$), $k_\perp$	5 W/m-K
Thermal conductivity (//), $k_{//}$	50 W/m-K
Heat capacity, C_p	0.710 J/g-K
Thermal diffusivity, α	0.032 cm^2/s
Stefan-Boltzman constant, σ	5.7×10^{-12} /sW/cm^2-K^4

C. Evaluation of MB-PFC's pumping capabilities

The MB-PFC operational parameter, ℓ_p/v, calculated from eq. (3) is plotted against particle flux in Fig. 2. The maximum fuel and impurity trapping capacities used are approximately 1.7 x 10^{16} DT-atoms/cm^2 and 4.2 x 10^{15} impurities/cm^2, respectively, averaged for Li, Be, and B at E = 100 eV. The operational space is illustrated by the space below the curves in this diagram. Two other cases where ℓ_p/L = 1/10 and 1/50 are also shown for comparison.

Under the conditions listed in Table 1: E = 100 eV, Γ_f= 1 x 10^{18} D,T/cm^2/s and Γ_i= 1 x 10^{18} C,O/cm^2/s, it is required for MB-PFCs to be able to pump these incoming particles that $\ell_p/v < 0.34$ for DT-particles and $\ell_p/v < 4.2$ for C, O-impurities, using the diagram in Fig. 2. As such, the requirement for DT-fuel particle pumping generally covers that for impurity gettering. For example, the case study condition in Table 1: ℓ_p/v = 0.25 meets both the requirements. It is thus possible to operate one module for two purposes.

However, modular application allows us to operate two MB-PFCs: one for impurities and the other for DT-fuel pumping under two different conditions. This capability is particularly important if a specific gettering material and/or specific temperature are required. For example, helium gettering requires nickel coatings [7] which may not be the best for DT-fuel particle pumping.

The throughput speed of the MB-PFC module in this case study, having the plasma exposure size of 50 cm x 100 cm, is 1.5 x 10^2 Torr ℓ/s for DT-particles. Only ten of these modules can meet the requirement for ITER: 1.5 x 10^3 Torr ℓ/s. Here, the belt temperature must be maintained lower than 500 °C for effective particle control. This will be shown to be possible in the next section.

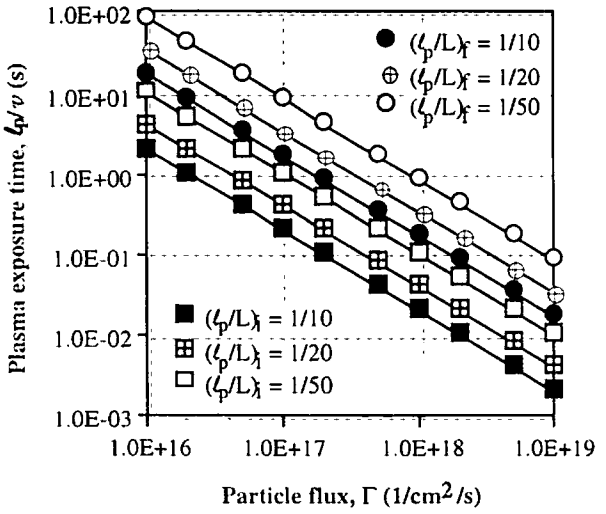

Fig. 2 MB-PFC operational space diagram as to ℓ_p/v, plotted against particle fluxes for different ℓ_p/L. Two sets of curves are illustrated: the subscripts of i and f indicate impurity and fuel, respectively.

III. MB-PFC MODULE FOR HEAT REMOVAL AND TEMPERATURE CONTROL

Temperature control is important for all belt modules in order to prevent material degradation and to maintain proper particle control. In addition, modules designed specifically for power conversion must operate at high temperature for efficient energy recovery.

The need to remove heat under vacuum conditions raises special concerns. Previously, we examined three possible mechanisms for heat removal in a vacuum or low-pressure heat exchanger: contact conductance, thermal radiation, and impinging liquid jets. Radiation heat transfer possesses clear operational advantages but is compatible only with temperatures above 800 – 1000°C. Operation in this range allows not only effective heat removal, but also the possibility of energy conversion with efficiency of 50% or more. Below 800°C, contact conductance has been shown to easily transfer the required heat loads even at low temperature [3].

In this work the limits of heat removal from a moving belt divertor have been quantified in both the exposure zone and heat exchanger. The maximum heat flux and total energy removed by the belt depends on the maximum allowable temperature as well as the maximum allowable belt speed. In order to avoid the belt materials erosion due to radiation-enhanced sublimation, we have restricted the maximum surface temperature to 1000°C. In this regime, radiation from the exposed belt surface to the first wall (~0.1 MW/m^2) can be neglected since it is much less than the incident heat flux. A belt temperature much higher than 1000°C would not offer substantial improvement, and may complicate material selection in the heat exchanger.

The maximum belt speed depends on the belt drive system, which uses vacuum rollers for direction and speed control. In order to minimize the forces on the tensioning system and prevent excessive belt stretching and erosion, a limit of 2 m/s is imposed. This is a soft limit, which can be further refined through experimentation.

A. Exposure Zone

The maximum local surface temperature strongly depends on the local peak heat flux. A general heat flux profile is defined using a Gaussian profile (with characteristic width λ) on top of a constant base (q_o), in order to allow us to examine the effect of peaking while maintaining the average heat input ($<q_p>$) constant:

$$q_p'' = q_o(1 + fe^{-(x/\lambda)^2}) \qquad (6)$$

$$q_o = < q_p > \frac{\ell_p}{\ell_p + f\lambda\sqrt{\pi}} \qquad (7)$$

Here ℓ_p is the heated length (plasma-exposed length), f is the peaking factor, and x is measured with respect to the

center of the Gaussian. This heat flux was used as a boundary condition on the energy equation expressed in a coordinate system moving with the belt speed:

$$\frac{d^2T}{dx^2} = \frac{1}{\alpha}\frac{dT}{dt} \qquad (8)$$

Equation 8 neglects parallel conduction along the belt direction of position, which is valid if $\alpha/v\ \ell_p < 1$. Even with a significantly enhanced parallel belt conductivity of 50 W/m-K, this ratio is still of the order of 3×10^{-5}.

Figure 3 shows an example of the non-dimensional temperature along the exposed belt surface *vs.* non-dimensional time, $t^* = (t_b^2/\alpha)\, t$, for f = 2 and λ = 5 cm, with T^* defined by:

$$T^* = (< q_p > t_b / k_1) T \qquad (9)$$

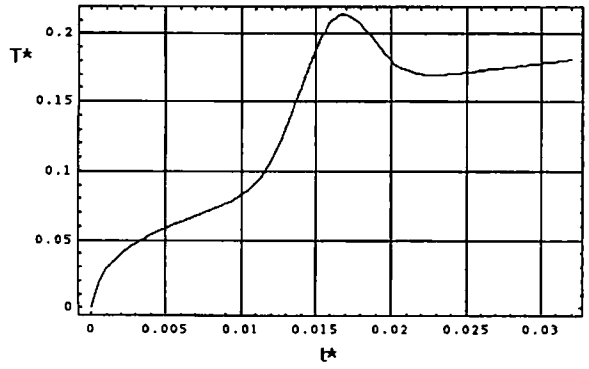

Fig. 3. Surface temperature with peaking factor = 2

Figure 4 shows the maximum surface temperature as a function of local peaking for λ = 5 cm. The maximum surface temperature occurs at the exit until the peaking exceeds ~1. For low values of peaking, the maximum surface temperature actually drops because heat is allowed to diffuse more deeply in the belt before reaching the exit. Above a peaking factor of 2, the local heat flux dominates, and the maximum temperature reaches an asymptotic value

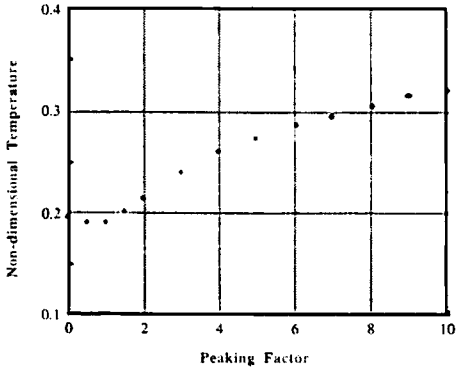

Fig. 4. Maximum surface temperature vs. local peaking.

of $T^* \sim 0.4$ when the heat flux is a pure Gaussian. For <q> = 2 MW/m^2, this asymptotic value corresponds with a surface temperature ~ 800°C higher than the inlet temperature. More moderate values of peaking in the range of 2 – 4 would give 400 – 500 ° C temperature rise, which could be reduced most easily by increasing the belt velocity.

B. Radiation Heat Exchanger

The high-temperature heat exchanger concept is shown in Figure 5. It utilizes a multi-pass approach to provide a compact system with adequate heat transfer area. He coolant is used due to the high operating temperature. One of the advantages of MB-PFC is its ability to remove heat at such high temperature that thermal conversion efficiency in excess of 50% is possible. We set a minimum coolant outlet temperature of 700 – 800°C to capitalize on this capability. This minimum belt temperature provides adequate radiation heat transfer to keep the heat exchanger surface area modest. With the resulting average belt temperature rise of 200 – 300 ° C, the belt thickness should be at least 3 mm.

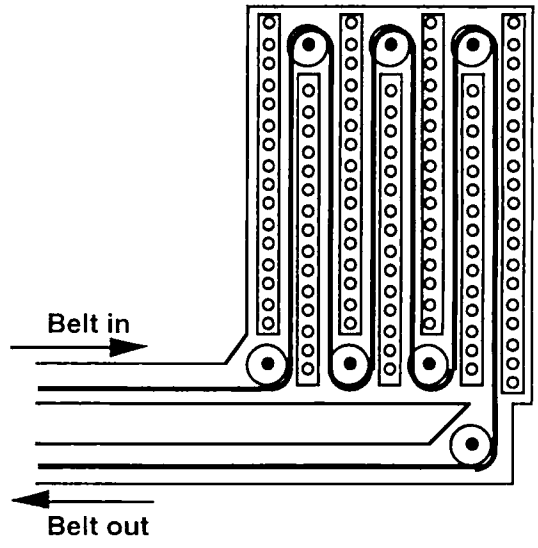

Fig. 5. Radiation heat exchanger schematic design

A counter-flow heat exchanger was analyzed for these conditions, including thermal resistance in the coolant walls and film. The governing equations are energy balance in the belt and coolant:

$$q_{HX}'' = \sigma\varepsilon(T_b^4 - T_s^4)$$
$$= -\rho_b v_b C_{pb} t_b \frac{dT_b}{dx} = \rho_h v_h C_{ph} t_h \frac{dT_h}{dx} \qquad (10)$$

where subscripts "b", "s", and "h" refer to the belt, coolant channel surface and helium coolant, respectively. The temperature difference between the coolant channel surface and bulk coolant are determined from:

$$T_s - T_h = q_{HX}''\left(\frac{d_s}{k} + \frac{1}{h}\right) \qquad (11)$$

Results are shown in Figure 6 for a He outlet temperature of 700°C, chosen to allow a high-temperature He Brayton cycle with thermal conversion efficiency > 45%.

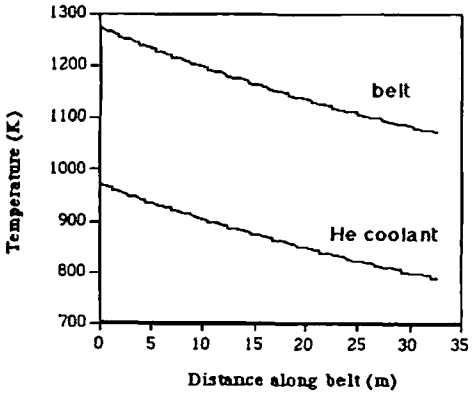

Fig. 6. Belt and He temperatures in heat exchanger.

C. Contact Heat Exchanger

Contact conductance (h_C) depends strongly on the contact pressure, background gas pressure, and surface characteristics (*e.g.*, roughness and microhardness). A contact conductance of ~5000 W/m^2, which is possible even in vacuum, appears adequate. The contact area, A, to remove 1 MW of power with a 50°C temperature difference is calculated to be only 4 m^2, using the relation:

$$q_{total} = h_c A \Delta T . \qquad (12)$$

A contact heat transfer scheme probably will require coolant flow through rotating seals, which is a complication but appears practical.

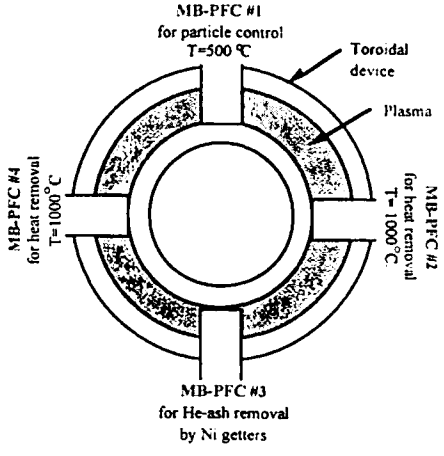

Fig. 7 An example of modular application of MB-PFCs.

CONCLUSION

It is never possible to direct completely the particle and heat flows into toroidally discontinuous MB-PFC modules. However, these MB-PFCs can act as the drains to remove particles and heat from a steady-state fusion system. In this report, we have demonstrated the possibility that particle control and heat removal can be done by two or more MB-PFC modules, as shown in Fig. 7, operating under respective optimum conditions. These operating conditions have been analyzed, taking advantage of several key features of MB-PFC that are not found in other PFC concepts using liquid metal [8] or particulate free flows [9].

ACKNOWLEDGMENT

This work has been supported by the U. S. Department of Energy, Office of Fusion Energy Sciences.

REFERENCES

1. R. Parker et al., "Plasma-Wall Interactions in ITER", *J. Nucl. Mater.* **241-243**(1997)1-26.

2. B. LaBombard et al., "Experimental Investigation of Transport Phenomena in the Scrape-Off Layer and Divertor", *J. Nucl. Mater.* **241-243**(1997)149-166.

3. Y. Hirooka, M. S. Tillack and A. Grossman, "Steady-State Impurity Control, Heat Removal and Tritium Recovery by Moving-Belt Plasma-Facing Components", Proc. 17th IEEE Symp. on Fusion Engineering, San Diego, Oct. 6-9, 1997, p. 906-909.

4. J.P. Biersack and W. Eckstein, "Sputtering Studies with the Monte Carlo Program TRIM.SP", *Appl. Phys.* **A34**(1984)73-94.

5. R. W. Conn, "Pumped divertors and limiters for tokamaks, *Fusion Eng. Design* **14**(1991)81-97.

6. R. A. Causey, "The Interaction of Tritium with Graphite and its Impact on Tokamak Operations", *J. Nucl. Mater.* **162-164**(1989)151-161.

7. J. N. Brooks, "The TEXTOR helium self-pumping experiment: design, plans and supporting ion-beam data on helium retention in Nickel" *J. Nucl. Mater.* **176&177**(1990)635-639.

8. B. Badger et al., "UWMAK-I, A Wisconsin Toroidal Fusion Reactor Design", *University of Wisconsin Report*: UWFDM-68, 1974.

9. K. Ikuta and A. Miyahara, "A Moving Toroidal Limiter", *J. Nucl. Mater.* **121**(1884)374-377.